All-optical coherent quantum-noise cancellation in cascaded optomechanical systems

Jakob Schweer,[1] Daniel Steinmeyer,[1] Klemens Hammerer,[2,1] and Michèle Heurs[1]

[1]*Institute for Gravitational Physics and Max Planck Institute for Gravitational Physics (Albert Einstein Institute), Leibniz Universität Hannover, Callinstraße 38, 30167 Hannover, Germany*

[2]*Institute for Theoretical Physics, Leibniz Universität Hannover, Appelstraße 2, 30167 Hannover, Germany*

(Received 5 August 2022; accepted 9 September 2022; published 28 September 2022)

Coherent quantum-noise cancellation (CQNC) can be used in optomechanical sensors to surpass the standard quantum limit (SQL). In this paper, we investigate an optomechanical force sensor that uses the CQNC strategy by cascading the optomechanical system with an all-optical effective negative-mass oscillator. Specifically, we analyze matching conditions and losses and compare the two possible arrangements in which either the optomechanical or negative-mass system couples first to light. While both of these orderings yield a sub-SQL performance, we find that placing the effective negative-mass oscillator before the optomechanical sensor will always be advantageous for realistic parameters. The modular design of the cascaded scheme allows for better control of the subsystems by avoiding undesirable coupling between system components while maintaining a performance similar to the integrated configuration proposed earlier. We conclude our work with a case study of a micro-optomechanical implementation.

DOI: 10.1103/PhysRevA.106.033520

I. INTRODUCTION

Achieving force measurements at the quantum limit has been a significant focus for several decades [1,2] and has fueled the development of optomechanics [3–5]. Optomechanical sensors exploit the interaction of a light field with the motion of a mechanical oscillator to measure its displacement with high precision. Force measurements based on these schemes are subject to shot noise and quantum radiation-pressure back-action noise [6,7]. Shot noise is caused by the uncertainty in the number of photons over time and can be decreased relative to the signal by increasing the intensity of the optical field. In contrast, the back-action noise arises from the fluctuation in the radiation pressure of the optical field, which will increase with its intensity. The trade-off between these competing processes then sets a lower bound to the precision of the measurement, which is called the standard quantum limit (SQL) [7–9].

The SQL is not a fundamental limit, and many different approaches have been suggested to achieve measurements with sub-SQL accuracy. These approaches include frequency-dependent squeezing [10–12], variational measurements [13–15], dual mechanical resonators [16–19], and optical spring effects [20–22]. In essence, these ideas go beyond the SQL by measuring a quantum nondemolition (QND) variable of the probe, that is, a variable that commutes with itself for different moments in time. In a QND measurement, the back-action is transmitted to the canonically conjugate observable and thus avoided. A more general approach to QND measurements is gained by introducing another system that acts like a reference frame with an effective negative mass [23]. By measuring with respect to this reference system, a QND measurement is realized. When the reference system is a harmonic oscillator, an effective negative mass amounts to a negative eigenfrequency. This idea was first experimentally utilized in demonstrating Einstein-Podolsky-Rosen states of two atomic spin oscillators of positive and negative mass [24]. Based on this, back-action cancellation was demonstrated by Wasilewski *et al.* [25] in the context of magnetometry. Extending this idea, several proposals have been made in a hybrid setting of a mechanical oscillator and atomic spin ensembles [23,26], and the evasion of back-action noise in these spin ensembles was experimentally verified in [27]. Independently, Tsang and Caves [28,29] developed this idea in a more general context, called quantum-mechanics-free subsystems. In the context of optomechanics, the main idea is to introduce an "antinoise" path to the dynamics of the optomechanical sensor upon coupling to an ancillary resonator that acts as an effective negative mass. In this way, the back-action noise can be canceled coherently, and sub-SQL force sensing is achieved for all measurement frequencies. Appropriately, this approach is called coherent quantum-noise cancellation (CQNC). The details and experimental feasibility of this all-optical effective negative-mass oscillator were discussed in more detail by Wimmer *et al.* [30].

Within the area of CQNC force sensing, many other possible negative-mass oscillators and setups have been considered. Other setups include the use of ultracold atoms inside a separate cavity [31,32], hybrid optomechanical cavities (i.e., implementing an atomic ensemble inside the optomechanical sensor) [33,34], and employing Bose-Einstein

condensates [35]. Even a new all-optical setup was suggested using two detuned optical modes inside the force sensor [36]. These approaches can be categorized into integrated setups, where the effective negative mass is introduced directly into the optomechanical force sensor, and cascaded setups [37,38], where the effective negative-mass oscillator is a separate system. Recently, Zeuthen *et al.* [39] considered a broad class of effective negative-mass oscillators in a cascaded setting and even considered a possible coupling between the positive and negative-mass oscillator in a parallel topology.

Inspired by this, we want to discuss a cascaded version of the original all-optical setup [28,30]. Instead of implementing the antinoise path directly into the optomechanical sensor, an all-optical effective negative-mass oscillator is built as a separate system. The back-action is then canceled by coupling the force sensor to the effective negative-mass oscillator via a strong coherent field. This approach will give more freedom in the experimental design and simplify reaching the challenging conditions for a CQNC experiment. The main challenge before canceling quantum back-action noise is to measure the back-action noise. Due to the modular nature of the cascaded approach, this can be tackled entirely separately from the effective negative-mass oscillator. We will see that under some modifications to the matching conditions, our cascaded setup recovers the ideal CQNC performance described in [30], and the additional degrees of freedom from expanding the dimension of the system lead to different phenomena for sub-SQL force sensing. This includes the recovery of ideal CQNC around an off-resonant frequency and possible CQNC performance in the low- or high-frequency regime, even for unmatched CQNC conditions.

This paper is organized as follows. In Sec. II, we describe the model of our cascaded CQNC scheme and derive the quantum Langevin equations of motion. In Sec. III, we discuss force sensing in optomechanical sensors and derive the optimal parameters for ideal CQNC. In Sec. IV, we analyze possible deviations from the ideal conditions and their impact on the performance of coherent quantum-noise reduction. Then, in Sec. V, a case study is provided. Finally, we summarize our findings in Sec. VI.

II. MODEL

Figure 1(a) illustrates a possible schematic realization of our setup. We refer to [40] for details on the experimental implementation of all-optical CQNC. An optomechanical sensor (OMS), subject to an external force and radiation-pressure noise, is connected to an effective negative-mass oscillator (NMO) by a coherent light field. The force is then measured by detecting outgoing light after the second system. The order of subsystems can be chosen freely, and the two possible arrangements are depicted in Fig. 1(b). In the first case, the light travels through the NMO, followed by the OMS. We will refer to this case as NMO $\mapsto$ OMS. In the second case, the order is reversed; hence, the light will travel through the OMS first, and we will refer to this case as OMS $\mapsto$ NMO. The effects of these different arrangements on the performance of the back-action cancellation will be discussed later.

The OMS is modeled by an optical cavity with resonance frequency ω_{om}, containing a damped mechanical positive-

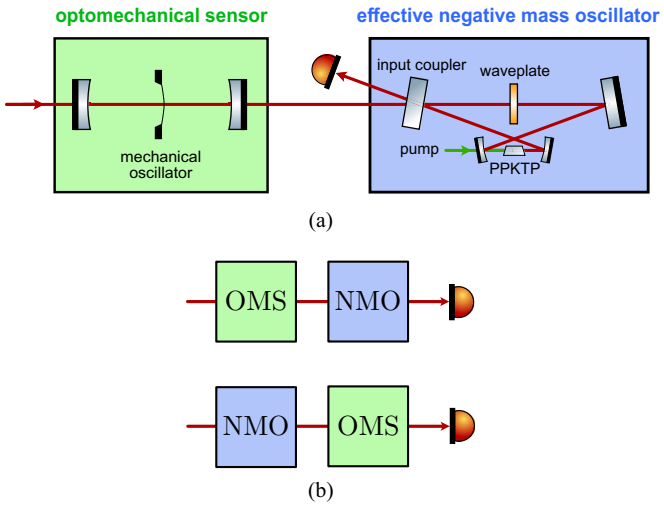

FIG. 1. (a) Sketch of the cascaded setup. The optomechanical sensor (green) consists of a mechanical oscillator inside an optical cavity, depicted in a membrane-in-the-middle setup. The effective negative-mass oscillator (blue) comprises two optical modes, coupled via a beam-splitter and down-conversion process. A nonlinear periodically poled potassium titanyl phosphate (PPKTP) crystal exemplifies the coupling for the down-conversion and a wave plate for the beam-splitter coupling. (b) Simplified depiction of the possible arrangements of the cascaded scheme.

mass oscillator (PMO) with resonance frequency ω_{m} and linewidth γ_{m}, coupled to the cavity field via radiation-pressure interaction and subjected to an external force F. Following the standard treatment of these force sensors [5], we move to a rotating frame with respect to the frequency ω_{L} of the strong driving laser field and arrive at the linearized Hamiltonian

$$H_{\mathrm{OMS}} = \Delta_{\mathrm{om}} c_{\mathrm{om}}^{\dagger} c_{\mathrm{om}} + \frac{\omega_{\mathrm{m}}}{2}\left(x_{\mathrm{m}}^2 + p_{\mathrm{m}}^2\right) + \frac{g x_{\mathrm{m}}}{\sqrt{2}}\left(c_{\mathrm{om}} + c_{\mathrm{om}}^{\dagger}\right). \tag{1}$$

Here, $\Delta_{\mathrm{om}} = \omega_{\mathrm{om}} - \omega_{\mathrm{L}}$ is the detuning of the optomechanical cavity to the incoming field, c_{om} ($c_{\mathrm{om}}^{\dagger}$) are the annihilation (creation) operators of the optical mode, and $x_{\mathrm{m}} = X/x_{\mathrm{ZPF}}$ and $p_{\mathrm{m}} = P x_{\mathrm{ZPF}}/\hbar$ are the position and momentum operators of the mechanical oscillator normalized to the zero-point fluctuation $x_{\mathrm{ZPF}} = \sqrt{\hbar/m\omega_{\mathrm{m}}}$, such that $[x_{\mathrm{m}}, p_{\mathrm{m}}] = i$. The last term in Eq. (1) describes the radiation-pressure interaction of the cavity mode and the mechanical oscillator. Its strength is given by $g = \sqrt{2}\omega_{\mathrm{c}} x_{\mathrm{ZPF}} \alpha_{\mathrm{c}}/L$, where L is the cavity length and $\alpha_{\mathrm{c}} \propto \sqrt{P}$ is the field amplitude of the cavity mode, proportional to the input power P. Introducing dimensionless amplitude and phase quadratures $c_{\mathrm{om}} = (x_{\mathrm{om}} + i p_{\mathrm{om}})/\sqrt{2}$, the Hamiltonian (1) implies the quantum Langevin equations (QLEs)

$$\dot{x}_{\mathrm{m}} = \omega_{\mathrm{m}} p_{\mathrm{m}}, \tag{2a}$$

$$\dot{p}_{\mathrm{m}} = -\omega_{\mathrm{m}} x_{\mathrm{m}} - \gamma_{\mathrm{m}} p_{\mathrm{m}} - g x_{\mathrm{om}} + \sqrt{\gamma_{\mathrm{m}}} F, \tag{2b}$$

$$\dot{x}_{\mathrm{om}} = -\frac{\kappa_{\mathrm{om}}}{2} x_{\mathrm{om}} + \Delta_{\mathrm{om}} p_{\mathrm{om}} + \sqrt{\kappa_{\mathrm{om}}} x_{\mathrm{om}}^{\mathrm{in}}, \tag{2c}$$

$$\dot{p}_{\mathrm{om}} = -\frac{\kappa_{\mathrm{om}}}{2} p_{\mathrm{om}} - \Delta_{\mathrm{om}} x_{\mathrm{om}} - g x_{\mathrm{m}} + \sqrt{\kappa_{\mathrm{om}}} p_{\mathrm{om}}^{\mathrm{in}}. \tag{2d}$$

Here, κ_{om} is the decay rate of the cavity mode, and $c_{\mathrm{om}}^{\mathrm{in}} = (x_{\mathrm{om}}^{\mathrm{in}} + i p_{\mathrm{om}}^{\mathrm{in}})/\sqrt{2}$ is its vacuum input noise. The noise pro-

cess fulfills $\langle c_{\rm om}^{\rm in}(t) c_{\rm om}^{\rm in\dagger}(\tau)\rangle = \delta(t-\tau)$. In Eq. (2) we have defined the scaled force operator $F = \mathrm{F}/\sqrt{\hbar m \gamma_{\rm m} \omega_{\rm m}}$ with dimension $\sqrt{\mathrm{Hz}}$. It consists of the to-be-detected force signal $F_{\rm sig}$ acting on the mechanical oscillator and Brownian thermal noise $F_{\rm th}$ of the oscillator. The scaled thermal noise satisfies $\langle F_{\rm th}(t) F_{\rm th}(\tau)\rangle = n_{\rm th}\delta(t-\tau)$, where $n_{\rm th} = k_B T/\hbar\omega_{\rm m}$ is the average phonon number of the mechanical oscillator.

The NMO consists of two optical modes $c_{\rm c}$ and a, with resonance frequencies $\omega_{\rm c}$ and $\omega_{\rm a}$, coupled with a beam-splitter and down-conversion process. In analogy to [30,40], we refer to $\omega_{\rm c}$ as the meter cavity and $\omega_{\rm a}$ as the ancilla cavity. The Hamiltonian of this system (see Appendix A for details) is given by

$$H_{\rm NMO} = \Delta_{\rm c} c_{\rm c}^\dagger c_{\rm c} + \Delta_{\rm a} a^\dagger a + g_{\rm BS}(a c_{\rm c}^\dagger + a^\dagger c_{\rm c}) + g_{\rm DC}(a c_{\rm c} + a^\dagger c_{\rm c}^\dagger), \tag{3}$$

with the detunings $\Delta_{\rm c,a} = \omega_{\rm c,a} - \omega_{\rm L}$, the beam-splitter coupling strength $g_{\rm BS}$, and the coupling strength of the down-conversion process $g_{\rm DC}$. As above, we introduce amplitude and phase quadratures associated with the meter and ancilla cavity. Then the Hamiltonian (3) implies the following QLEs for the NMO:

$$\dot{x}_{\rm c} = -\frac{\kappa_{\rm c}}{2} x_{\rm c} + \Delta_{\rm c} p_{\rm c} + (g_{\rm BS} - g_{\rm DC}) p_{\rm a} + \sqrt{\kappa_{\rm c}} x_{\rm c}^{\rm in}, \tag{4a}$$

$$\dot{p}_{\rm c} = -\frac{\kappa_{\rm c}}{2} x_{\rm c} - \Delta_{\rm c} x_{\rm c} - (g_{\rm BS} + g_{\rm DC}) x_{\rm a} + \sqrt{\kappa_{\rm c}} p_{\rm c}^{\rm in}, \tag{4b}$$

$$\dot{x}_{\rm a} = -\frac{\kappa_{\rm a}}{2} x_{\rm a} + \Delta_{\rm a} p_{\rm a} + (g_{\rm BS} - g_{\rm DC}) p_{\rm c} + \sqrt{\kappa_{\rm a}} x_{\rm a}^{\rm in}, \tag{4c}$$

$$\dot{p}_{\rm a} = -\frac{\kappa_{\rm a}}{2} p_{\rm a} - \Delta_{\rm a} x_{\rm a} - (g_{\rm BS} + g_{\rm DC}) x_{\rm c} + \sqrt{\kappa_{\rm a}} p_{\rm a}^{\rm in}, \tag{4d}$$

with the cavity linewidths $\kappa_{\rm c}$ and $\kappa_{\rm a}$ and the input noise processes $a^{\rm in}$ and $c_{\rm c}^{\rm in}$. Under the condition $g_{\rm BS} - g_{\rm DC} = 0$, the QLEs (4) generate an interaction similar to that in Eqs. (2). Additionally, driving the meter cavity on resonance $\Delta_{\rm c} = 0$ results in $\Delta_{\rm a} = \omega_{\rm a} - \omega_{\rm c}$. Thus, the detuning between the meter and ancilla cavity can be used to generate an effective negative-mass oscillator.

III. FORCE SENSING AND IDEAL CQNC

To solve the dynamics of both systems, we turn to the frequency domain. Introducing the Fourier domain operators

$$O(\omega) = \frac{1}{\sqrt{2\pi}} \int \mathrm{d}t\, O(t) e^{i\omega t},$$

Eqs. (2)–(4) can be solved using the standard input-output formalism [41]

$$x^{\rm out} = \sqrt{\kappa} x - x^{\rm in}, \tag{5}$$

$$p^{\rm out} = \sqrt{\kappa} p - p^{\rm in}. \tag{6}$$

We consider the systems separately, first the OMS. On resonance, $\Delta_{\rm om} = 0$, the output quadratures read

$$x_{\rm om}^{\rm out} = e^{i\phi} x_{\rm om}^{\rm in},$$
$$p_{\rm om}^{\rm out} = e^{i\phi} p_{\rm om}^{\rm in} - \chi_{\rm m} g^2 \kappa_{\rm om} \chi_{\rm om}^2 x_{\rm om}^{\rm in} + \chi_{\rm m} \sqrt{\kappa_{\rm om}} g \chi_{\rm om} \sqrt{\gamma_{\rm m}} F, \tag{7}$$

where $e^{i\phi} = (\frac{\kappa_{\rm om}}{2} - i\omega)/(\frac{\kappa_{\rm om}}{2} + i\omega)$. We have defined the susceptibilities for the optomechanical cavity and the mechanical oscillator as

$$\chi_{\rm om}(\omega) = \left[i\omega + \frac{\kappa_{\rm om}}{2} \right]^{-1}, \tag{8}$$

$$\chi_{\rm m}(\omega) = \omega_{\rm m} \left[\left(\omega^2 - \omega_{\rm m}^2\right) - i\gamma_{\rm m}\omega \right]^{-1}. \tag{9}$$

The mechanical oscillator is susceptible to the external force F, which contains the force signal $F_{\rm sig}$ and thermal noise $F_{\rm th}$. By measuring with light, the force signal can be estimated via a phase measurement, which also introduces additional noise due to the radiation pressure. From the measured phase $p_{\rm om}^{\rm out}$ in Eq. (7) we can give an unbiased estimator $\hat{F}$ of the force F as

$$\hat{F} = \frac{1}{\sqrt{\gamma_{\rm m}} \chi_{\rm m}\, g\sqrt{\kappa_{\rm om}} \chi_{\rm om}} p_{\rm om}^{\rm out} = F + F_{\rm add}, \tag{10}$$

where the additional force noise, added by the measurement light, is defined as

$$F_{\rm add} = F_{\rm th} + \frac{e^{i\phi}}{\sqrt{\gamma_{\rm m}} \chi_{\rm m}\, g\sqrt{\kappa_{\rm om}} \chi_{\rm om}} p_{\rm om}^{\rm in} - \frac{g\sqrt{\kappa_{\rm om}} \chi_{\rm om}}{\sqrt{\gamma_{\rm m}}} x_{\rm om}^{\rm in}. \tag{11}$$

To characterize the sensitivity of the force measurement, we use the (power) spectral density of the added noise, defined by

$$S_F(\omega)\delta(\omega - \omega') = \tfrac{1}{2}(\langle F_{\rm add}(\omega) F_{\rm add}(-\omega')\rangle + \mathrm{c.c.}). \tag{12}$$

Assuming uncorrelated amplitude and phase quadratures, the added-noise spectral density is

$$S_F = \frac{k_B T}{\hbar\omega_{\rm m}} + \frac{1}{2 G_{\rm om} \gamma_{\rm m} |\chi_{\rm m}|^2} + \frac{G_{\rm om}}{2\gamma_{\rm m}}, \tag{13}$$

where we defined the frequency-dependent measurement strength as

$$G_{\rm om}(\omega) = g^2 \kappa_{\rm om} |\chi_{\rm om}(\omega)|^2 = \Gamma_{\rm om} \frac{\left(\frac{\kappa_{\rm om}}{2}\right)^2}{\omega^2 + \left(\frac{\kappa_{\rm om}}{2}\right)^2}, \tag{14}$$

with a Lorentzian shape and maximum $\Gamma_{\rm om} = \frac{4g^2}{\kappa_{\rm om}}$. In this form, the noise spectral density (13) is dimensionless. To arrive at a force-noise spectral density in units of N^2/Hz, one has to rescale it such that $S_F(\omega) = \hbar m \gamma_{\rm m} \omega_{\rm m} S_F(\omega)$ for a given optomechanical force sensor [30]. The terms in Eq. (13) are thermal noise due to Brownian motion of the mechanical oscillator (first term), shot noise in the phase quadrature (second term), and back-action noise from the amplitude quadrature (third term). The thermal noise adds a flat background to the force sensitivity, which is independent of the measurement rate $G_{\rm om}$ and frequency. Throughout this paper, we will assume that the thermal noise either is dominated by back-action noise [30] or is suppressed by cooling of the mechanical mode and therefore neglect this term.

The shot noise term is proportional to the inverse of the measurement rate $G_{\rm om}$ and thus proportional to the inverse of the power, as $G_{\rm om} \propto P$. Additionally, the back-action noise is proportional to $G_{\rm om}$. This implies that an optimal power value, which minimizes Eq. (13), exists for each frequency.

Minimizing Eq. (13) with respect to $G_{\rm om}$ for all frequencies gives the achievable lower bound

$$S_F(\omega) \geqslant \frac{1}{\gamma_m|\chi_{\rm m}(\omega)|} \equiv S_{\rm SQL}(\omega), \tag{15}$$

which is the SQL. The optimal measurement rate required is

$$G_{\rm SQL}(\omega) = \frac{1}{|\chi_{\rm m}(\omega)|}. \tag{16}$$

Next, we consider the NMO. On resonance, $\Delta_{\rm c} = 0$, and for $g_{\rm BS} = g_{\rm DC} = \frac{1}{2}g_{\rm a}$ the output quadratures read

$$\begin{aligned} x_{\rm c}^{\rm out} &= e^{i\theta}x_{\rm c}^{\rm in}, \\ p_{\rm c}^{\rm out} &= e^{i\theta}p_{\rm c}^{\rm in} - \chi_{\rm a}g_{\rm a}^2\kappa_{\rm c}\chi_{\rm c}^2 x_{\rm c}^{\rm in} \\ &\quad + \chi_{\rm a}\sqrt{\kappa_{\rm c}}g_{\rm a}\chi_{\rm c}\sqrt{\kappa_{\rm a}}\left(\frac{\kappa_{\rm a}/2 + i\omega}{\Delta_{\rm a}}x_{\rm a}^{\rm in} + p_{\rm a}^{\rm in}\right), \end{aligned} \tag{17}$$

where $e^{i\theta} = (\frac{\kappa_{\rm c}}{2} - i\omega)/(\frac{\kappa_{\rm c}}{2} + i\omega)$. We have defined susceptibilities of the meter cavity $\chi_{\rm c}$ and the ancilla cavity $\chi_{\rm a}$ as

$$\chi_{\rm c} = \left[i\omega + \frac{\kappa_{\rm c}}{2}\right]^{-1}, \tag{18}$$

$$\chi_{\rm a} = \Delta_{\rm a}\left[\left(\omega^2 - \Delta_{\rm a}^2 - \frac{\kappa_{\rm a}^2}{4}\right) - i\kappa_{\rm a}\omega\right]^{-1}. \tag{19}$$

The aim of our setup is to couple the two systems in a manner that the back-action noise in the force spectrum will cancel, hence allowing for a sub-SQL performance. In our dual-cavity setup, this is done by cascading the two systems and matching the parameters of the NMO accordingly.

As seen in Fig. 1(b), the whole scheme has two possible arrangements. Thus, to cascade the systems, we choose $x_{\rm c}^{\rm out} = x_{\rm om}^{\rm in}$ and $p_{\rm c}^{\rm out} = p_{\rm om}^{\rm in}$ for the case NMO $\mapsto$ OMS and $x_{\rm om}^{\rm out} = x_{\rm c}^{\rm in}$ and $p_{\rm om}^{\rm out} = p_{\rm c}^{\rm in}$ for OMS $\mapsto$ NMO. For ideal CQNC, the order will not matter. We will discuss cases that depend on the order further below. After cascading the two systems, we can again identify the additional force noise as in Eq. (10) and derive the added noise spectral density

$$\begin{aligned} S_F &= \frac{1}{2G_{\rm om}\gamma_{\rm m}|\chi_{\rm m}|^2} \\ &\quad + \frac{G_{\rm a}^2|\chi_{\rm a}|^2 + G_{\rm om}^2|\chi_{\rm m}|^2 + 2\,G_{\rm a}G_{\rm om}{\rm Re}(\chi_{\rm m}\chi_{\rm a}^*)}{2G_{\rm om}\gamma_{\rm m}|\chi_{\rm m}|^2} \\ &\quad + \frac{G_{\rm a}\kappa_{\rm a}|\chi_{\rm a}|^2}{2G_{\rm om}\gamma_{\rm m}|\chi_{\rm m}|^2}\left(\frac{\omega^2 + \kappa_{\rm a}^2/4}{\Delta_{\rm a}^2} + 1\right); \end{aligned} \tag{20}$$

see Appendix B for details. Like we did for the measurement strength of the OMS in Eq. (14), we have defined the frequency-dependent measurement strength of the NMO,

$$G_{\rm a}(\omega) = g_{\rm a}^2\kappa_{\rm c}|\chi_{\rm c}(\omega)|^2 = \Gamma_{\rm a}\,\frac{\left(\frac{\kappa_{\rm c}}{2}\right)^2}{\omega^2 + \left(\frac{\kappa_{\rm c}}{2}\right)^2}, \tag{21}$$

with $\Gamma_{\rm a} = \frac{4g_{\rm a}^2}{\kappa_{\rm c}}$. The terms in Eq. (20) are the shot noise (first term), back-action noise (second term), and shot noise from the ancilla cavity (last term). The back-action noise is then canceled if the conditions are such that

$$g_{\rm BS} = g_{\rm DC} = \frac{1}{2}g_{\rm a}, \tag{22}$$

$$G_{\rm om}(\omega) = G_{\rm a}(\omega), \tag{23}$$

$$\chi_{\rm m}(\omega) = -\chi_{\rm a}(\omega) \tag{24}$$

for all ω. This means that the ancilla cavity should couple to the light with the same strength as the PMO, but the response to the force signal should be opposite to the PMO; hence, it behaves as an effective negative mass. Considering the explicit form of Eqs. (9) and (19), condition (24) entails further restrictions:

(1) The detuning of the ancilla cavity to the meter cavity is

$$\Delta_{\rm a} = -\omega_{\rm m}, \tag{24a}$$

which effectively moves the ancilla cavity to the negative-mass frame.

(2) The linewidth of the ancilla cavity $\kappa_{\rm a}$ should match the damping rate of the mechanical oscillator

$$\kappa_{\rm a} = \gamma_{\rm m} \tag{24b}$$

to mimic the oscillating behavior of the PMO.

(3) The susceptibilities $\chi_{\rm m}$ and $\chi_{\rm a}$ differ by a factor $\kappa_{\rm a}^2/4$. To alleviate this, the detuning $|\Delta_{\rm a}| \gg \kappa_{\rm a}$, and together with the forgoing points, this implies the resolved sideband limit of the ancilla cavity.

$$\omega_{\rm m} \gg \kappa_{\rm a}, \tag{24c}$$

and a large quality factor of the mechanical oscillator,

$$Q_{\rm m} = \frac{\omega_{\rm m}}{\gamma_{\rm m}} \gg 1. \tag{24d}$$

These conditions are similar to the integrated setup [30], but instead of the coupling strengths $g_{\rm a}$ and g, the measurement strengths $G_{\rm a}$ and $G_{\rm om}$ need to match.

Assuming conditions (22)–(24) are met, the back-action term in Eq. (20) will vanish, and we arrive at

$$S_F = \frac{1}{2G_{\rm om}\gamma_{\rm m}|\chi_{\rm m}|^2} + \frac{1}{2}\left(\frac{\omega^2 + \gamma_{\rm m}^2/4}{\omega_{\rm m}^2} + 1\right), \tag{25}$$

which contains only shot-noise contributions of the measured phase quadrature and the ancilla cavity. The contribution of the OMS is sometimes referred to as the fundamental quantum limit [9], energetic quantum limit [42], or the quantum Cramér-Rao bound [43–45]. In the limit of large measurement strength, we arrive at the lower bound

$$S_F(\omega) \geqslant \frac{1}{2}\left(\frac{\omega^2 + \gamma_{\rm m}^2/4}{\omega_{\rm m}^2} + 1\right) \equiv S_{\rm CQNC}(\omega). \tag{26}$$

Combining Eqs. (15) and (26), we find

$$S_{\rm CQNC} = S_{\rm SQL} \times \frac{1}{2Q_{\rm m}}\left(\frac{\omega^2 + \gamma_{\rm m}^2/4 + \omega_{\rm m}^2}{\sqrt{\left(\omega^2 - \omega_{\rm m}^2\right)^2 + \gamma_{\rm m}^2\omega^2}}\right). \tag{27}$$

Thus, for $Q_{\rm m} \gg 1$, we can summarize

$$S_{\rm CQNC} = S_{\rm SQL} \times \begin{cases} 1 & \text{on resonance } \omega = \omega_{\rm m}, \\ 1/(2Q_{\rm m}) & \text{off resonance } \omega \lessgtr \omega_{\rm m}. \end{cases} \tag{28}$$

In conclusion, under the additional condition that $G_{\rm om} = G_{\rm a}$, the cascaded setup reproduces the same findings as in [30],

TABLE I. Parameters of the optomechanical sensor used in Figs. 2–5.

Parameter		Normalized value	Value
$\omega_{\rm m}$	mechanical resonance frequency	1	500 kHz
$\gamma_{\rm m}$	mechanical linewidth	$10^{-3}\,\omega_{\rm m}$	500 Hz
$Q_{\rm m}$	mechanical quality factor	$\frac{\omega_{\rm m}}{\gamma_{\rm m}}$	1000
$\kappa_{\rm om}$	optomechanical cavity linewidth	$10\,\omega_{\rm m}$	5 MHz

leading to an enhancement in performance up to a factor of $2Q_{\rm m}$ off resonance and SQL performance on resonance.

IV. IMPERFECT CQNC

Conditions (22)–(24) are the ideal case for a perfect cancellation of back-action noise and will not be satisfied in an actual experiment. Therefore, we will discuss possible imperfections and their impact on the performance of our cascaded scheme. These imperfections include mismatches to the parameters in Eqs. (22)–(24) and possible losses. Another degree of freedom of our setup is the order in which the light passes through the subsystems (i.e., NMO $\mapsto$ OMS or OMS $\mapsto$ NMO), but this will affect the force-sensing only for imperfections that directly affect the force signal. Hence, we split our discussion into order-dependent and -independent categories. Data shown in the figures in this section refer to an OMS given by the parameters in Table I.

A. Order-independent imperfections

The parameters discussed in this section will impede the cancellation of back-action noise and, as a result, limit the CQNC performance but will not affect the force signal. Hence, the possible CQNC performance in the face of these imperfections will not depend on the system order.

1. Nonideal ancilla cavity linewidth $\kappa_{\rm a} \neq \gamma_{\rm m}$

The strictest requirement for an all-optical CQNC setup is to match the ancilla cavity linewidth to the damping rate of the mechanical oscillator. Assume that all conditions for ideal CQNC are matched, except $\kappa_{\rm a} \neq \gamma_{\rm m}$. Since the measurement strengths $G_{\rm om} = G_{\rm a}$ are matched for all frequencies and we assume no propagation losses in the system, this effectively reduces to the integrated CQNC setup [30]. The spectral density of added noise (20) in this case becomes

$$S_F = \frac{1}{2G_{\rm om}\gamma_{\rm m}|\chi_{\rm m}|^2} + \frac{G_{\rm om}}{2\gamma_{\rm m}}\left|\frac{\chi_{\rm m}+\chi_{\rm a}}{\chi_m}\right|^2 + \frac{\kappa_{\rm a}|\chi_{\rm a}|^2}{2\gamma_{\rm m}|\chi_{\rm m}|^2}\left(\frac{\omega^2+\kappa_{\rm a}^2/4}{\omega_{\rm m}^2}+1\right). \tag{29}$$

For an optimal $G_{\rm om}$, we find the minimal spectral density for the added noise,

$$S_F = \frac{|\chi_{\rm m}+\chi_{\rm a}|}{\gamma_{\rm m}|\chi_{\rm m}|} + \frac{\kappa_{\rm a}|\chi_{\rm a}|^2}{2\gamma_{\rm m}|\chi_{\rm m}|^2}\left(\frac{\omega^2+\kappa_{\rm a}^2/4}{\omega_{\rm m}^2}+1\right). \tag{30}$$

This is composed of measurement shot and back-action noise (first term) and noise introduced by the ancilla cavity (second term). The second term will dominate the first one for frequencies off resonance, setting a bound to the achievable performance. The ratio between the spectral density (30) and the SQL is

$$S_F = \frac{\kappa_{\rm a}}{2\,\omega_{\rm m}} \times S_{\rm SQL} \tag{31}$$

for $\kappa_{\rm a} < \omega_{\rm m}$. For $\kappa_{\rm a} \gg \omega_{\rm m}$, the effect of CQNC will vanish for low frequencies, converging to the SQL, while for large frequencies, the added noise is larger than the SQL. This is illustrated in Fig. 2.

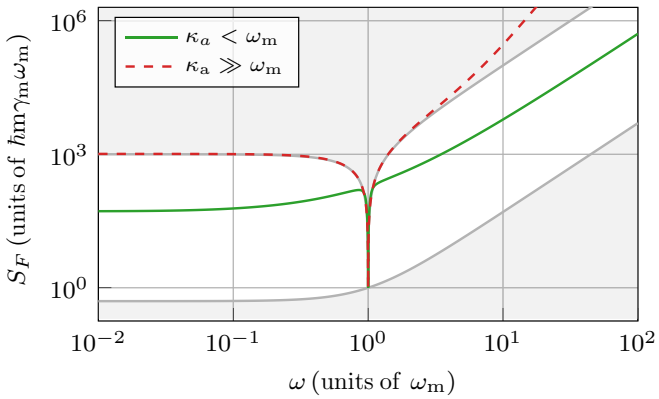

FIG. 2. Force noise for a mismatch between the ancilla cavity linewidth $\kappa_{\rm a}$ and the damping rate of the mechanical oscillator $\gamma_{\rm m}$. For $\kappa_{\rm a} < \omega_{\rm m}$ an improvement of $\kappa_{\rm a}/2\omega_{\rm m}$ can be achieved off resonance (solid green line). For $\kappa_{\rm a} \gg \omega_{\rm m}$, the effect of CQNC is completely canceled for low frequencies, and the sensitivity is worse than the SQL for high frequencies (red dashed line). The shaded areas mark the bounds for sub-SQL sensitivity, from below the fundamental limit given by Eq. (26) and from above the SQL given by Eq. (15). Parameters are given in Table I.

2. Unequal measurement strengths $G_{\rm om} \neq G_{\rm a}$

Next, we consider a mismatch of the measurement strengths $G_{\rm a} \neq G_{\rm om}$ while matching the other CQNC conditions. This entails unmatched cavity linewidth $\kappa_{\rm c} \neq \kappa_{\rm om}$ and unmatched couplings $g_{\rm a} \neq g$. Introducing parameters for the linewidth mismatch $\kappa_{\rm c} = \epsilon\,\kappa_{\rm om}$ and coupling mismatch $g_{\rm a} = \sqrt{\delta}g$, we find for the spectral density

$$S_F = \frac{1}{2G_{\rm om}\gamma_{\rm m}|\chi_{\rm m}|^2} + \frac{G_{\rm om}}{2\gamma_{\rm m}}\left|1-\delta\epsilon\frac{|\chi_{\rm c}|^2}{|\chi_{\rm om}|^2}\right|^2 + \delta\epsilon\frac{|\chi_{\rm c}|^2}{|\chi_{\rm om}|^2}\frac{1}{2}\left(\frac{\omega^2+\gamma_{\rm m}^2/4}{\omega_{\rm m}^2}+1\right). \tag{32}$$

For suitable couplings g and cavity linewidth κ, we can find a frequency at which the back-action term in Eq. (32) will vanish, and ideal CQNC is possible. This is the case when the Lorentzians $G_{\rm a}$ and $G_{\rm om}$ are such that they will intersect at a frequency $\omega \neq 0$. We find that

$$\omega_* = \pm\sqrt{\frac{\delta\,\epsilon-\epsilon^2}{1-\delta\,\epsilon}\frac{\kappa_{\rm om}}{2}} \tag{33}$$

is a real-valued frequency for the following parameters:

$$g_{\rm a} = g \quad \Rightarrow \quad \kappa_{\rm c} < \kappa_{\rm om} \quad \text{or} \quad \kappa_{\rm c} > \kappa_{\rm om}, \tag{34a}$$

$$g_{\rm a} < g \quad \Rightarrow \quad \epsilon > \frac{1}{\delta} \quad \text{or} \quad \epsilon < \delta, \tag{34b}$$

$$g_a > g \quad \Rightarrow \quad \epsilon > \delta \quad \text{or} \quad \epsilon < \frac{1}{\delta}. \tag{34c}$$

Consequently, a cavity linewidth mismatch can compensate for every possible matching condition of the couplings, and ideal CQNC can be achieved at ω_*.

For nonvanishing back-action, we can again minimize the spectral density (32) with an optimal $G_{\rm om}$. Turning to the low-frequency limit ($\kappa_{\rm c,om} \gg \omega$), the measurement strengths become frequency independent, $G_{\rm om,a} \to \Gamma_{\rm om,a}$, and the ratio $|\chi_{\rm c}|^2/|\chi_{\rm om}|^2 \to 1/\epsilon^2$. The minimal noise spectral density is then

$$S_F = \left|1 - \frac{\delta}{\epsilon}\right| \times S_{\rm SQL} + \left(\frac{\delta}{\epsilon}\right) \times S_{\rm CQNC}. \tag{35}$$

Ideal CQNC can be recovered for $\epsilon = \delta$, which means $\Gamma_{\rm om} = \Gamma_{\rm a}$. Hence, as long as the rate at which the back-action information leaks out of the system is matched, ideal CQNC is possible.

For the converse case ($\kappa_{\rm c,om} \ll \omega$) the cavity susceptibilities $|\chi_{\rm c}|^2 \approx |\chi_{\rm om}|^2$, effectively canceling in Eq. (32). The optimal spectral density becomes

$$S_F = |1 - \delta\,\epsilon| \times S_{\rm SQL} + (\delta\,\epsilon) \times S_{\rm CQNC}. \tag{36}$$

In this case, ideal CQNC can be recovered for $\delta = 1/\epsilon$, which entails $g_{\rm a}^2\kappa_c = g^2\kappa_{\rm om}$. We depict our main findings in Fig. 3.

We also considered a combination of the imperfections discussed in this section. If, for example, $G_{\rm om} \neq G_{\rm a}$ and, additionally, $\kappa_{\rm a} \neq \gamma_{\rm m}$, the noise spectral density will be a combination of Eqs. (29) and (32). In this case, the cancellation of back-action noise is possible for the cases discussed above, but the ancilla cavity noise floor is higher because of the linewidth mismatch $\gamma_{\rm m} \neq \kappa_{\rm a}$. Thus, our findings will remain

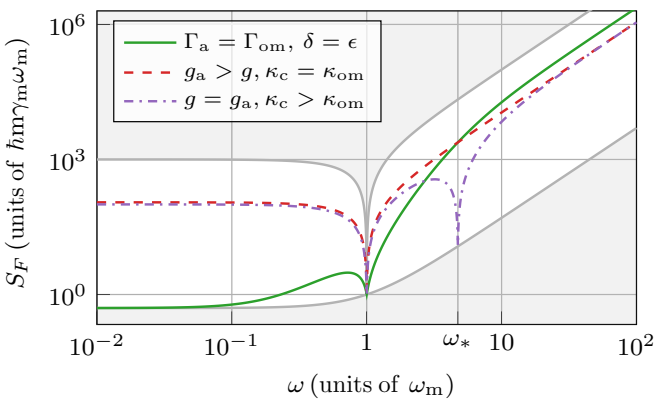

FIG. 3. Force noise for imperfect matching of measurement strength. For mismatched coupling strength compensated by linewidth mismatch, perfect noise cancellation can be recovered at low frequencies (solid green line for $\epsilon = \delta = 0.9$). For matched linewidth but mismatched coupling strength, noise cancellation is limited, but sub-SQL performance is possible (dashed red line for $\delta = 0.9$). In the case of matched coupling strength but mismatched linewidth, we find a frequency (33) where perfect noise cancellation is possible (dash-dotted purple line, with $\epsilon = 0.9$). The shaded areas mark the bounds for sub-SQL sensitivity, from below the fundamental limit given by Eq. (26) and from above the SQL given by Eq. (15). Parameters are given in Table I.

the same, but the achievable performance off resonance is given by the noise spectral density (31).

B. Order-dependent imperfections

The parameters discussed in this section, namely, losses, not only hamper the cancellation of back-action noise but also affect the force signal directly.

1. Losses

We first consider propagation losses, which occur between the first and second systems. The propagation losses are modeled by mixing the output signal of the first system with vacuum in a beam-splitter-like interaction. This leads to a modified output signal [8],

$$x'_{\rm out} = \sqrt{\eta}\, x_{\rm out} + \sqrt{1-\eta}\, x_{\rm vac}, \tag{37}$$

where $x_{\rm vac}$ represents the vacuum field and $\eta \in [0, 1]$ is the efficiency of the process. Due to this additional noise, information about the back-action interaction of the first system is lost to the vacuum; hence, perfect cancellation of back-action noise is not possible. As before, we can find an optimal coupling strength to minimize the additional noise. For the system order NMO $\mapsto$ OMS, we achieve a minimal spectral density off resonance,

$$S_F = \sqrt{1-\eta} \times S_{\rm SQL}. \tag{38}$$

In the opposite order OMS $\mapsto$ NMO, in addition to the loss of back-action information, some force signal will be lost due to propagation losses. Hence, the added noise will increase for this topology. We find

$$S_F = \frac{\sqrt{1-\eta}}{\eta} \times S_{\rm SQL} \tag{39}$$

for the minimal spectral density off resonance. The spectral density is increased by $1/\eta$ compared to the case NMO $\mapsto$ OMS and hence directly proportional to the lost force signal. Losses after the second system constitute the detection efficiency and can be modeled similarly. Since this will not affect the cancellation of back-action noise, we will omit detection losses for now.

Apart from propagation losses, we take intracavity losses into account. Introducing a Markovian bath for each cavity, with coupling rates $\kappa_{\rm c}^{\rm bath}$ and $\kappa_{\rm om}^{\rm bath}$, the intracavity losses can be described in terms of the escape efficiencies

$$\eta_{\rm om,c}^{\rm esc} = \frac{\kappa_{\rm om,c}^{\rm in}}{\kappa_{\rm om,c}^{\rm in} + \kappa_{\rm om,c}^{\rm bath}} = \frac{\kappa_{\rm om,c}^{\rm in}}{\kappa_{\rm om,c}}. \tag{40}$$

Similar to propagation losses, introducing intracavity losses will always impede the cancellation of back-action noise, and depending on the order of the systems, the available force signal information will differ. For the case NMO $\mapsto$ OMS, with optimal measurement strength, we find the minimal spectral density

$$S_F = \frac{\sqrt{\eta_c^{\rm esc} + \eta_{\rm om}^{\rm esc} - 2\eta_c^{\rm esc}\eta_{\rm om}^{\rm esc}}}{\eta_{\rm om}^{\rm esc}} \times S_{\rm SQL}. \tag{41}$$

This encompasses both cases with propagation loss; for $\eta_{\rm om}^{\rm esc} \to 1$ we retrieve Eq. (38), and for $\eta_{\rm c}^{\rm esc} \to 1$ we get

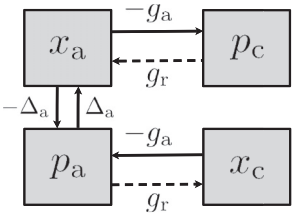

FIG. 4. Flow chart between the mode of the ancilla and the meter cavity. The solid line shows the original back-action flow, and the dashed line shows the noise introduced by the relative mismatch g_r of the beam-splitter and down-conversion coupling.

Eq. (39). Thus, for the configuration NMO ↦ OMS, the intracavity loss can be handled similarly to propagation loss.

For the case OMS ↦ NMO, we lose additional force signal due to intrinsic loss in the meter cavity. Moreover, the signal also picks up additional information about the phase quadrature. We arrive at the minimal spectral density,

$$S_F = \frac{\sqrt{\eta_c^{esc} + \eta_{om}^{esc} - 2\eta_c^{esc}\eta_{om}^{esc}}}{\eta_{om}^{esc}\,|1 - \eta_c^{esc}\kappa_c\chi_c|^2} \times S_{SQL}. \tag{42}$$

The term $|1 - \eta_c^{esc}\kappa_c\chi_c|^2$ describes the meter cavity's phase and noise contribution. Due to its dependence on the meter-cavity susceptibility χ_c, this difference is frequency dependent and will vanish for frequencies $\omega > \kappa_c$. For low frequencies, it will be at a maximal value of $|1 - 2\eta_c^{esc}|^2$, making intracavity losses extra punishing for the configuration OMS ↦ NMO. We see that introducing losses is detrimental to the possible noise reduction. As losses will never be avoidable, the system order NMO ↦ OMS should always be preferable since higher levels of noise reduction are achieved.

2. *Relative mismatch of g_{BS} and g_{DC}*

In addition to losses, a relative mismatch between the beam-splitter coupling g_{BS} and down-conversion coupling g_{DC} will also affect the noise cancellation depending on the system order. So far, we have assumed $g_{BS} = g_{DC} = 1/2\, g_a$ in order to mimic the back-action interaction of the OMS. We will now fix $g_{BS} + g_{DC} = g$ and introduce a mismatch between the beam-splitter and down-conversion couplings

$$\frac{g_{BS} - g_{DC}}{g_{BS} + g_{DC}} = g_r \neq 0. \tag{43}$$

As shown in Fig. 4, the relative mismatch g_r allows the phase quadratures to couple back into the amplitude quadrature and thus deviate from the back-action interaction of the OMS. This introduces a noise path and will limit the cancellation of back-action noise. It also affects the force noise differently for the different system orders. For the case OMS ↦ NMO, the force signal is imprinted on the output phase quadrature of the OMS, and with the introduced mismatch, it is possible for the signal to couple to the amplitude quadrature. In contrast, for NMO ↦ OMS, the force signal will remain fully in the output phase quadrature. Thus, this results in different spectral noise densities for our phase measurement. For general mismatches, this will not reduce to a simple expression. The resulting spectral densities were calculated numerically and are shown in Fig. 5. The CQNC performance is limited for low

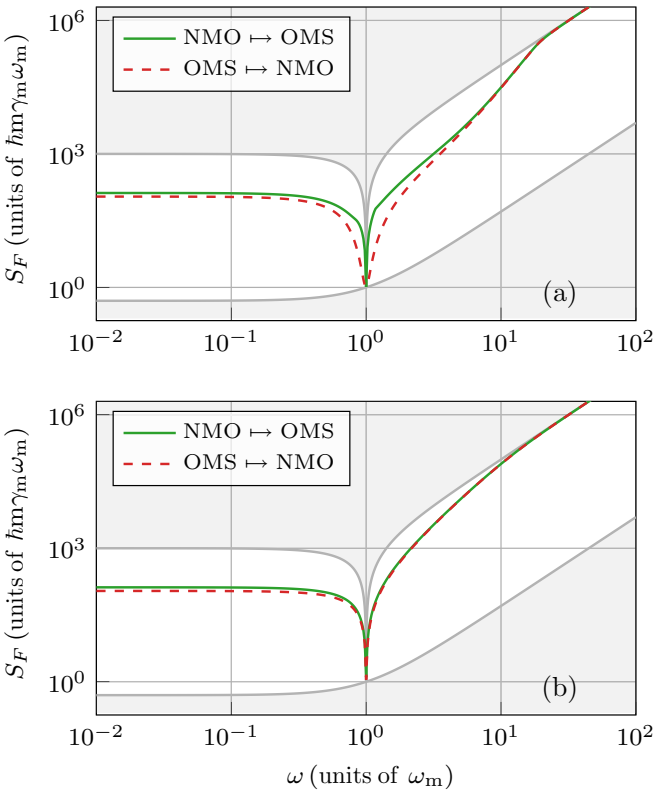

FIG. 5. Force noise for relative mismatch of beam-splitter and down-conversion coupling (a) for $g_r = 0.2$ and (b) for $g_r = -0.2$. The relative mismatch introduces additional noise by modifying the effective back-action term of the NMO. Perfect noise cancellation is not possible, but sub-SQL levels are achievable for low frequencies. For high frequency, no noise reduction is possible. Traversing through the OMS first seems advantageous for noise cancellation. The shaded areas mark the bounds for sub-SQL sensitivity, from below the fundamental limit given by Eq. (26) and from above the SQL given by Eq. (15). Parameters are given in Table I.

frequencies, but sub-SQL levels are still possible. Contrary to losses, the order OMS ↦ NMO seems advantageous for a relative mismatch of the couplings. CQNC will vanish entirely in the high-frequency limit, and no sub-SQL performance is possible.

V. CASE STUDY

After discussing ideal CQNC and the most relevant deviations from the ideal parameters, we now turn to a realistic situation one would expect in an actual experiment. For an integrated setup, reasonable parameters were discussed in [30], which were revised in [40] for a cascaded setup, and two reasonable sets of parameters were given. From there, we found a different set of parameters which achieve broadband noise reduction for frequencies below the mechanical resonance of the oscillator. Losses are of particular interest in our case study, as they influence the noise reduction depending on the system order. Our set of parameters is shown in Table II.

The OMS must be limited by quantum back-action noise to measure the possible cancellation of back-action noise. For this, the quantum back-action noise in Eq. (13) must be

TABLE II. Proposed set of parameters.

Parameter		Normalized value	Value/2π
ω_{m}	mechanical resonance frequency	1	500 kHz
γ_{m}	mechanical linewidth	$10^{-8}\,\omega_{\mathrm{m}}$	5 mHz
κ_{c}	meter-cavity linewidth	$4\,\omega_{\mathrm{m}}$	2 MHz
Δ_{a}	ancilla cavity detuning	$-0.99\,\omega_m$	−495 kHz
κ_{a}	ancilla cavity linewidth	$\frac{2}{5}\,\omega_{\mathrm{m}}$	200 kHz
g_{BS}	beam-splitter coupling strength	$1.01\,\frac{g}{2}$	253 kHz
g_{DC}	down-conversion coupling strength	$0.97\,\frac{g}{2}$	243 kHz
$\eta_{\mathrm{c}}^{\mathrm{esc}}$	escape efficiency NMO	0.9	
κ_{om}	optomechanical cavity linewidth	$0.99\,\kappa_{\mathrm{c}}$	1.98 MHz
g	optomechanical coupling strength	ω_m	500 kHz
$\eta_{\mathrm{om}}^{\mathrm{esc}}$	escape efficiency OMS	0.9	
η_{prop}	propagation efficiency	0.97	
η_{det}	detection efficiency	0.97	

much larger than the thermal noise. In the low-frequency limit ($\kappa_{\mathrm{om}} \gg \omega$), this can be expressed in terms of the quantum cooperativity as

$$C_{\mathrm{q}} = \frac{\Gamma_{\mathrm{om}}}{\gamma_{\mathrm{m}}}\frac{\hbar\,\omega_{\mathrm{m}}}{k_B T} = \frac{4g^2\hbar}{\kappa_{\mathrm{om}} k_B T}\,Q_{\mathrm{m}} \gg 1. \tag{44}$$

Modern silicon nitride membranes have exceeded quality factors of $Q_{\mathrm{m}} = 10^8$ [46]; thus, the OMS would be quantum back-action limited for a temperature $T = 4$ K, a temperature achievable with cryogenics. For higher temperatures, the quality factor must be increased to elevate the back-action effects over the thermal noise floor, and similarly, lower temperatures allow for a lower quality factor. In order to account for this and compare all OMSs of frequency ω_{m}, once they can resolve the quantum back-action, we normalize our force noise by the quality factor Q_{m}.

Matching most parameters, such as ancilla cavity detuning Δ_{a} and the cavity linewidth κ_{c} and κ_{om}, should not be a problem; we assume they are closely matched. More delicate to match are the coupling strengths. A down-conversion coupling of $g_{\mathrm{DC}} = 2\pi \times 250$ kHz and a beam-splitter coupling of $g_{\mathrm{BS}} \geqslant 2\pi \times 235$ kHz were readily achieved [40]; thus, we set the optomechanical coupling strength to $g = 2\pi \times 500$ kHz. Optomechanical coupling strengths of $g = 2\pi \times 440$ kHz have been reported in micromechanical setups [27], and higher couplings on the order of megahertz should be possible [47]. Hence, our assumed coupling strength should be reasonable. If these levels cannot be reached for the optomechanical coupling strength, one could still compensate for this mismatch by the cavity linewidths, as described in Eq. (30), and increase the performance for low frequencies.

For a negative-mass oscillator, where the two modes are not spatially separated, as depicted in Fig. 1(a), the escape efficiency will also dictate the achievable linewidth of the ancilla cavity. An escape efficiency of 90% should be achievable [48], which, with a meter-cavity linewidth of $\kappa_{\mathrm{c}} = 2$ MHz, makes an ancilla cavity linewidth of $\kappa_{\mathrm{a}} = 200$ kHz possible. For the OMS, similar escape efficiencies should be achievable. Detection efficiencies over 97% were already realized [49]. Similarly, propagation losses between the systems should not be an issue. We assume 3% losses from both propagation and detection.

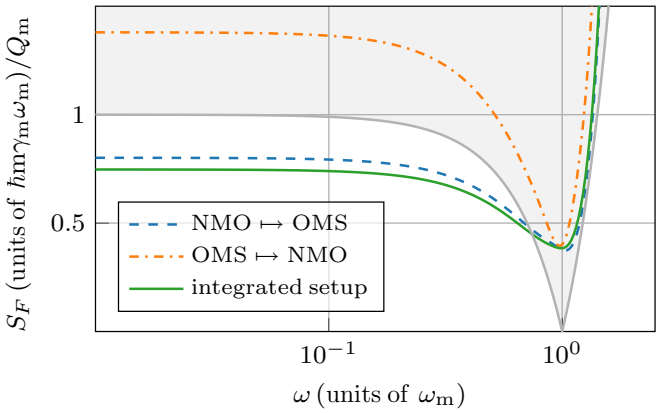

FIG. 6. Force noise normalized to Q_{m} for the parameters given by Table II and temperature $T = 4$ K. For low frequencies, sub-SQL performance is possible for the integrated setup (solid green line) and the case NMO ↦ OMS (dashed blue line). No sub-SQL levels are possible for the case OMS ↦ NMO (dash-dotted orange line). The shaded area shows levels above the SQL.

The achievable sensitivities for the parameters in Table II are shown in Fig. 6. In the low-frequency regime, the configuration NMO ↦ OMS shows a reduction of 20% below the SQL and results almost comparable to the integrated setup. No sub-SQL sensitivity can be achieved for the other system order, OMS ↦ NMO. This is not surprising, as we saw in Sec. IV B that this configuration suffers additional penalties from losses. We see that instead of matching the parameters (22)–(24), the limiting factor for noise reduction in a realistic case will be losses. Additionally, as losses will never be entirely avoidable, choosing the right system ordering, NMO ↦ OMS, is of utmost importance.

VI. CONCLUSION

In this work, we discussed a cascaded version of the all-optical coherent quantum-noise-cancellation setup proposed by Tsang and Caves [28,30]. Instead of introducing the antinoise path directly into the optomechanical cavity, we considered an all-optical effective negative-mass oscillator as a stand-alone system and removed the back-action noise of the positive-mass oscillator by coupling both systems coherently via a strong drive field. Under the conditions (22)–(24), we then rediscovered the perfect cancellation of back-action noise. Afterwards, we discussed deviations from the ideal conditions, including losses and the influence of the system order. We saw that for mismatched measurement strengths, by choosing the cavity linewidth and coupling strength in a specific way, CQNC can be recovered in the high- or low-frequency regime or even at a specific frequency $\omega_* \neq \omega_{\mathrm{m}}$. For losses and a relative mismatch of beam-splitter and down-conversion coupling, the system order will also affect the noise-cancellation performance. Finally, we discussed the performance of our setup for a set of realistic parameters and showed that a quantum-noise reduction of 20% below the SQL is possible for the order NMO ↦ OMS in the low-frequency regime.

ACKNOWLEDGMENTS

We thank J. Junker and B. Schulte for fruitful discussions regarding the experimental setup. This research was funded by the Deutsche Forschungsgemeinschaft (Excellence Cluster QuantumFrontiers (EXC 2123 Project ID 390837967), SFB 1227 (DQ-mat, project A05), GRK 1991) and the Quantum- and Nano-Metrology (QUANOMET) initiative from VW-Vorab (ZN3294).

APPENDIX A: DETAILS ON THE HAMILTONIAN H_{NMO}

Here, we give some more details on the Hamiltonian H_{NMO} in Eq. (3). The effective negative-mass oscillator consists of two optical modes with different frequencies ω_{c} and ω_{a}, coupled by a beam-splitter and down-conversion process. The whole Hamiltonian reads

$$H_{\mathrm{NMO}} = H_0 + H_{\mathrm{drive}} + H_{\mathrm{DC}} + H_{\mathrm{BS}}, \tag{A1}$$

where the first term represents the free Hamiltonian of the optical modes,

$$H_0 = \omega_{\mathrm{c}} c_{\mathrm{c}}^\dagger c_{\mathrm{c}} + \omega_{\mathrm{a}} a^\dagger a. \tag{A2}$$

The second term describes the laser drive, which drives the meter-cavity mode c_{c}, and is given by

$$H_{\mathrm{drive}} = iE(e^{-i\omega_{\mathrm{L}} t} c_{\mathrm{c}}^\dagger - e^{i\omega_{\mathrm{L}} t} c_{\mathrm{c}}). \tag{A3}$$

Here, ω_{L} denotes the laser frequency, and E describes the laser-field amplitude, which is given by $|E| = \sqrt{\kappa_{\mathrm{c}} P/\hbar\omega_{\mathrm{L}}}$, with the laser power P and cavity linewidth κ_{c}. The third term describes a two-mode squeezing process. In this, a pump field impinges on a nonlinear crystal, and a pump photon of frequency ω_{P} is converted into two photons of lower frequency. In the usual treatment of such processes, the pump is assumed to be a strong coherent field. In a rotating frame with respect to the pump frequency and linearized pump field [50], the Hamiltonian is then

$$H_{\mathrm{DC}} = g_{\mathrm{DC}}(a c_{\mathrm{c}} + a^\dagger c_{\mathrm{c}}^\dagger). \tag{A4}$$

The coupling strength of the down-conversion process is given by $g_{\mathrm{DC}} = \Gamma l \frac{c}{L}$, where l is the length of the crystal, L is the cavity length, c is the speed of light, and Γ is the gain parameter. We refer to [30,51] for more details on the gain parameter. The last term describes the beam-splitter interaction. It is given by

$$H_{\mathrm{BS}} = g_{\mathrm{BS}}(a^\dagger c_{\mathrm{c}} + c_{\mathrm{c}}^\dagger a), \tag{A5}$$

where g_{BS} denotes the coupling strength of this process. For a generic beam splitter, the strength is defined by $g_{\mathrm{BS}} = rc/L$, with r being the reflectivity of the beam splitter. Alternatively, for the setup considered in Fig. 1(a), where the two modes are not spatially separated, the beam-splitter interaction can be achieved with a wave plate [40]. The strength is then given by

$$g_{\mathrm{BS}} = \frac{c}{L}\frac{\theta}{2}\sin 2\tau, \tag{A6}$$

with θ being the wave plate angle and τ being the delay. Moving to a rotating frame with respect to the laser frequency ω_{L} and assuming a strong driving field, the Hamiltonian can be linearized, and we arrive at Eq. (3).

APPENDIX B: CALCULATION OF NOISE SPECTRAL DENSITIES

We consider a general linear quantum system consisting of n system variables, k inputs and outputs, and m bath variables. The input-output relations can be written as

$$\mathbf{x}_{\mathrm{out}} = K_{\mathrm{in}}^\top \mathbf{x} - \mathbf{x}_{\mathrm{in}}, \tag{B1}$$

with a vector $\mathbf{x}$ containing the n system variables and $\mathbf{x}_{\mathrm{in}}$ and $\mathbf{x}_{\mathrm{out}}$ vectors for the k inputs and outputs. The whole system is governed by the equations of motion

$$\dot{\mathbf{x}}(t) = M_{\mathrm{sys}}\mathbf{x}(t) + K_{\mathrm{in}}\mathbf{x}_{\mathrm{in}}(t) + K_{\mathrm{bath}}\mathbf{x}_{\mathrm{bath}}(t), \tag{B2}$$

where we have introduced the system matrix M_{sys} and input matrices K_{in} and K_{bath} for the input and bath quadratures. The equations of motion (B2) can be solved in the Fourier domain, where $\dot{\mathbf{x}}(t) = i\omega\mathbf{x}(\omega)$. It follows that

$$\mathbf{x} = (i\omega\mathbb{1} - M_{\mathrm{sys}})^{-1}(K_{\mathrm{in}}\mathbf{x}_{\mathrm{in}} + K_{\mathrm{bath}}\mathbf{x}_{\mathrm{bath}}). \tag{B3}$$

Together with Eq. (B1), we derive the output quadratures as

$$\begin{aligned}\mathbf{x}_{\mathrm{out}} &= K_{\mathrm{in}}^\top \mathbf{x} - \mathbf{x}_{\mathrm{in}} \\ &= \left(K_{\mathrm{in}}^\top (i\omega\mathbb{1} - M_{\mathrm{sys}})^{-1} K_{\mathrm{in}} - \mathbb{1}\right)\mathbf{x}_{\mathrm{in}} \\ &\quad + K_{\mathrm{in}}^\top (i\omega\mathbb{1} - M_{\mathrm{sys}})^{-1} K_{\mathrm{bath}}\mathbf{x}_{\mathrm{bath}} \\ &= T_{\mathrm{in}}\mathbf{x}_{\mathrm{in}} + T_{\mathrm{bath}}\mathbf{x}_{\mathrm{bath}} \\ &= \mathcal{T}\,\tilde{\mathbf{x}}_{\mathrm{in}},\end{aligned} \tag{B4}$$

where

$$\tilde{\mathbf{x}}_{\mathrm{in}} = \begin{pmatrix}\mathbf{x}_{\mathrm{in}} \\ \mathbf{x}_{\mathrm{bath}}\end{pmatrix}, \tag{B5}$$

$$\mathcal{T} = (T_{\mathrm{in}}, T_{\mathrm{bath}}). \tag{B6}$$

From this, we can calculate the (symmetrized) spectral density matrix as

$$\begin{aligned}\delta(\omega-\omega')S_{\mathrm{out}}(\omega) &= \tfrac{1}{2}\langle \mathbf{x}_{\mathrm{out}}(\omega)\mathbf{x}_{\mathrm{out}}^\dagger(\omega')\rangle + \mathrm{c.c.} \\ &= \tfrac{1}{2}\langle \mathcal{T}(\omega)\tilde{\mathbf{x}}_{\mathrm{in}}\tilde{\mathbf{x}}_{\mathrm{in}}^\dagger\mathcal{T}^\dagger(-\omega')\rangle + \mathrm{c.c.} \\ &= \tfrac{1}{2}\langle \mathcal{T}(\omega)S_{\mathrm{in}}\mathcal{T}^\dagger(-\omega')\rangle + \mathrm{c.c.},\end{aligned} \tag{B7}$$

with S_{in} being the input spectral density matrix. Every subsystem in our setup has four system variables. Hence, the system matrices M_{sys} and bath input matrices K_{bath} are all 4×4 dimensional. The input and output variables are the two quadratures of the laser light, making the input matrices K_{in} 4×2 dimensional.

To model losses, the output quadratures are mixed with vacuum noise via a beam-splitter interaction, which are then

$$\mathbf{x}'_{\mathrm{out}} = \underbrace{\begin{pmatrix}1&0&0&0\\0&1&0&0\end{pmatrix}\eta_{4\times 4}\begin{pmatrix}\mathcal{T}&0\\0&\mathbb{1}\end{pmatrix}}_{\mathcal{T}_{\mathrm{loss}}}\begin{pmatrix}\tilde{\mathbf{x}}_{\mathrm{in}}\\ \mathbf{x}_{\mathrm{vac}}\end{pmatrix}. \tag{B8}$$

The second matrix mixes the cavity output with vacuum, and the first matrix is the partial trace over the lost output port of the beam splitter.

Finally, we need to cascade the two subsystems. For this we choose $\mathbf{x}_{\text{in},2} = \mathbf{x}'_{\text{out},1}$, where subscripts 1 and 2 stand for the first and second systems. The total output quadratures are then given by

$$\mathbf{x}'_{\text{out},2} = \mathcal{T}_2^{\text{loss}} \begin{pmatrix} \mathcal{T}_1^{\text{loss}} & 0 & 0 \\ 0 & \mathbb{1}_{4\times4} & 0 \\ 0 & 0 & \mathbb{1}_{2\times2} \end{pmatrix} \begin{pmatrix} \mathbf{x}_{\text{in}} \\ \mathbf{x}_{\text{bath},1} \\ \mathbf{x}_{\text{vac},1} \\ \mathbf{x}_{\text{bath},2} \\ \mathbf{x}_{\text{vac},2} \end{pmatrix} = \mathcal{T}_{\text{total}} \mathbf{x}_{\text{in,total}}. \tag{B9}$$

The equations of motion (2) for the optomechanical sensor imply the following matrices:

$$M_{\text{sys}}^{\text{OMS}} = \begin{pmatrix} -\frac{\kappa_{\text{om}}}{2} & \Delta_{\text{om}} & 0 & 0 \\ -\Delta_{\text{om}} & -\frac{\kappa_{\text{om}}}{2} & -g & 0 \\ 0 & 0 & 0 & \omega_{\text{m}} \\ -g & 0 & -\omega_{\text{m}} & -\gamma_{\text{m}} \end{pmatrix}, \tag{B10a}$$

$$K_{\text{in}}^{\text{OMS}} = \begin{pmatrix} \sqrt{\kappa_{\text{om}}^{\text{in}}} & 0 \\ 0 & \sqrt{\kappa_{\text{om}}^{\text{in}}} \\ 0 & 0 \\ 0 & 0 \end{pmatrix}, \tag{B10b}$$

$$K_{\text{bath}}^{\text{OMS}} = \begin{pmatrix} \sqrt{\kappa_{\text{om}}^{\text{bath}}} & 0 \\ 0 & \sqrt{\kappa_{\text{om}}^{\text{bath}}} \\ 0 & 0 \\ 0 & \sqrt{\gamma_{\text{m}}} \end{pmatrix}. \tag{B10c}$$

Similarly, the equations of motion (4) for the effective negative-mass oscillator imply

$$M_{\text{sys}}^{\text{NMO}} = \begin{pmatrix} -\frac{\kappa_{\text{c}}}{2} & \Delta_{\text{c}} & 0 & (g_{\text{BS}} - g_{\text{DC}}) \\ -\Delta_{\text{c}} & -\frac{\kappa_{\text{c}}}{2} & -(g_{\text{BS}} + g_{\text{DC}}) & 0 \\ 0 & (g_{\text{BS}} - g_{\text{DC}}) & -\frac{\kappa_{\text{a}}}{2} & \Delta_{\text{a}} \\ -(g_{\text{BS}} + g_{\text{DC}}) & 0 & -\Delta_{\text{a}} & -\frac{\kappa_{\text{a}}}{2} \end{pmatrix}, \tag{B11a}$$

$$K_{\text{in}}^{\text{NMO}} = \begin{pmatrix} \sqrt{\kappa_{\text{c}}^{\text{in}}} & 0 \\ 0 & \sqrt{\kappa_{\text{c}}^{\text{in}}} \\ 0 & 0 \\ 0 & 0 \end{pmatrix}, \tag{B11b}$$

$$K_{\text{bath}}^{\text{NMO}} = \begin{pmatrix} \sqrt{\kappa_{\text{c}}^{\text{bath}}} & 0 \\ 0 & \sqrt{\kappa_{\text{c}}^{\text{bath}}} \\ \sqrt{\kappa_{\text{a}}} & 0 \\ 0 & \sqrt{\kappa_{\text{a}}} \end{pmatrix}. \tag{B11c}$$

From these expressions, we calculate the total transfer matrix in Eq. (B9), and together with the input spectral density,

$$S_{\text{in}} = \begin{cases} \frac{1}{2}\,\text{diag}(1,1,1,1,1,1,1,1,0,2S_F) & \text{for NMO} \mapsto \text{OMS}, \\ \frac{1}{2}\,\text{diag}(1,1,1,1,0,2S_F,1,1,1,1) & \text{for OMS} \mapsto \text{NMO}, \end{cases} \tag{B12}$$

we obtain the output spectral density with Eq. (B7). The spectral density of the added noise is then estimated from the phase component S_{out}^{pp} by dividing it by the coefficient of S_F.

[1] V. B. Braginsky, Y. I. Vorontsov, and K. S. Thorne, Science **209**, 547 (1980).

[2] V. B. Braginsky and F. Y. Khalili, *Quantum Measurement* (Cambridge University Press, Cambridge, 1995).

[3] P. Meystre, Ann. Phys. (Berlin, Ger.) **525**, 215 (2013).

[4] Y. Chen, J. Phys. B **46**, 104001 (2013).

[5] M. Aspelmeyer, T. J. Kippenberg, and F. Marquardt, Rev. Mod. Phys. **86**, 1391 (2014).

[6] C. M. Caves, Phys. Rev. Lett. **45**, 75 (1980).

[7] A. A. Clerk, M. H. Devoret, S. M. Girvin, F. Marquardt, and R. J. Schoelkopf, Rev. Mod. Phys. **82**, 1155 (2010).

[8] W. P. Bowen and G. J. Milburn, *Quantum Optomechanics* (CRC Press, Boca Raton, FL, 2020).

[9] S. L. Danilishin, F. Y. Khalili, and H. Miao, Living Rev. Relativ. **22**, 2 (2019).

[10] W. G. Unruh, in *Quantum Optics, Experimental Gravity, and Measurement Theory*, edited by P. Meystre and M. O. Scully (Springer, New York, 1983), pp. 647–660.

[11] R. S. Bondurant and J. H. Shapiro, Phys. Rev. D **30**, 2548 (1984).

[12] M. T. Jaekel and S. Reynaud, Europhys. Lett. **13**, 301 (1990).

[13] S. Vyatchanin and E. Zubova, Phys. Lett. A **201**, 269 (1995).

[14] H. J. Kimble, Y. Levin, A. B. Matsko, K. S. Thorne, and S. P. Vyatchanin, Phys. Rev. D **65**, 022002 (2001).

[15] F. Y. Khalili, Phys. Rev. D **81**, 122002 (2010).

[16] M. J. Woolley and A. A. Clerk, Phys. Rev. A **87**, 063846 (2013).

[17] T. Briant, M. Cerdonio, L. Conti, A. Heidmann, A. Lobo, and M. Pinard, Phys. Rev. D **67**, 102005 (2003).

[18] T. Caniard, P. Verlot, T. Briant, P. F. Cohadon, and A. Heidmann, Phys. Rev. Lett. **99**, 110801 (2007).

[19] L. M. de Lépinay, C. F. Ockeloen-Korppi, M. J. Woolley, and M. A. Sillanpää, Science **372**, 625 (2021).

[20] A. Buonanno and Y. Chen, Phys. Rev. D **64**, 042006 (2001).

[21] P. Verlot, A. Tavernarakis, T. Briant, P. F. Cohadon, and A. Heidmann, Phys. Rev. Lett. **104**, 133602 (2010).

[22] Y. Chen, S. L. Danilishin, F. Y. Khalili, and H. Müller-Ebhardt, Gen. Relativ. Gravity **43**, 671 (2011).

[23] E. S. Polzik and K. Hammerer, Ann. Phys. (Berlin, Ger.) **527**, A15 (2015).

[24] B. Julsgaard, A. Kozhekin, and E. S. Polzik, Nature (London) **413**, 400 (2001).

[25] W. Wasilewski, K. Jensen, H. Krauter, J. J. Renema, M. V. Balabas, and E. S. Polzik, Phys. Rev. Lett. **104**, 133601 (2010).

[26] K. Hammerer, M. Aspelmeyer, E. S. Polzik, and P. Zoller, Phys. Rev. Lett. **102**, 020501 (2009).

[27] C. B. Møller, R. A. Thomas, G. Vasilakis, E. Zeuthen, Y. Tsaturyan, M. Balabas, K. Jensen, A. Schliesser, K. Hammerer, and E. S. Polzik, Nature (London) **547**, 191 (2017).

[28] M. Tsang and C. M. Caves, Phys. Rev. Lett. **105**, 123601 (2010).

[29] M. Tsang and C. M. Caves, Phys. Rev. X **2**, 031016 (2012).

[30] M. H. Wimmer, D. Steinmeyer, K. Hammerer, and M. Heurs, Phys. Rev. A **89**, 053836 (2014).

[31] F. Bariani, H. Seok, S. Singh, M. Vengalattore, and P. Meystre, Phys. Rev. A **92**, 043817 (2015).

[32] T. Gebremariam, Y.-X. Zeng, M. Mazaheri, and C. Li, Sci. China Phys. Mech. Astron. **63**, 210311 (2019).

[33] A. Motazedifard, F. Bemani, M. H. Naderi, R. Roknizadeh, and D. Vitali, New J. Phys. **18**, 073040 (2016).

[34] S. K. Singh, M. Mazaheri, J.-X. Peng, and M. Asjad, arXiv:2201.10805.

[35] K. Zhang, P. Meystre, and W. Zhang, Phys. Rev. A **88**, 043632 (2013).

[36] J. Yan and J. Jing, Ann. Phys. (Berlin, Ger.) **533**, 2100119 (2021).

[37] H. J. Carmichael, Phys. Rev. Lett. **70**, 2273 (1993).

[38] C. W. Gardiner, Phys. Rev. Lett. **70**, 2269 (1993).

[39] E. Zeuthen, E. S. Polzik, and F. Y. Khalili, PRX Quantum **3**, 020362 (2022).

[40] D. Steinmeyer, Ph.D. thesis, Leibniz Universität Hannover, 2019.

[41] D. F. Walls and G. J. Milburn, *Quantum Optics*, 2nd ed. (Springer, Berlin, Heidelberg, 2007).

[42] V. B. Braginsky, M. L. Gorodetsky, F. Ya. Khalili, and K. S. Thorne, AIP Conf. Proc. **523**, 180 (2001).

[43] M. Tsang, H. M. Wiseman, and C. M. Caves, Phys. Rev. Lett. **106**, 090401 (2011).

[44] H. Miao, R. X. Adhikari, Y. Ma, B. Pang, and Y. Chen, Phys. Rev. Lett. **119**, 050801 (2017).

[45] F. Y. Khalili and E. Zeuthen, Phys. Rev. A **103**, 043721 (2021).

[46] D. Mason, J. Chen, M. Rossi, Y. Tsaturyan, and A. Schliesser, Nat. Phys. **15**, 745 (2019).

[47] R. A. Norte, J. P. Moura, and S. Gröblacher, Phys. Rev. Lett. **116**, 147202 (2016).

[48] J. Junker (private communication).

[49] H. Vahlbruch, M. Mehmet, K. Danzmann, and R. Schnabel, Phys. Rev. Lett. **117**, 110801 (2016).

[50] Z. Y. Ou, S. F. Pereira, and H. J. Kimble, Appl. Phys. B **55**, 265 (1992).

[51] R. L. Byer and R. L. Herbst, *Parametric Oscillation and Mixing* (Springer, Berlin, 1977), pp. 81–137.